Journal of Thermal Analysis and Calorimetry, Vol. 57 (1999) 875-881

CHARGE TRANSFER BETWEEN OXYGEN AND ZIRCONIA

A. Saiki[1], *H. Funakubo*[1], *N. Mizutani*[1], *K. Shinozaki*[1], *T. Bak*[2], *J. Nowotny*[2], *M. Rekas*[2] *and C. C. Sorrel*[2]

[1]Tokyo Institute of Technology, Department of Inorganic Materials O-okayama, Maguro-ku Tokyo, Japan
[2]Centre for Materials Research in Energy Conversion School of Materials Science and Engineering, The University of New South Wales Sydney, NSW 2052, Australia

Abstract

The extent of the surface charge, that develops during oxidation of zirconia, is determined using work function measurements for both bulk specimen and thin films. The bulk specimen of yttria-doped zirconia (10 mol%) exhibits maxima of the surface electrical effect at 373 and 973 K (130 and 280 mV, respectively) that can be considered in terms of oxygen chemisorption and oxygen non-stoichiometry. Thin film of undoped zirconia exhibits a maximum at 473 K (260 eV). Addition of yttria (10 mol%) to the thin film results in a substantial reduction of the maximum, to about 140 eV, that is shifted up to 600 K.

Keywords: charge transfer, Kelvin probe, oxidation, work function, zirconia

Introduction

Awareness is growing that performance of zirconia in electrochemical devices, such as solid oxide fuel cells, is determined by interfaces, such as surfaces and grain boundaries, rather than the bulk properties alone [1–4]. Consequently, the development of zirconia, that may exhibit enhanced performance in the devices, requires an increase in the present state of understanding on the local properties of interfaces and the impact of interfaces on functional properties of materials.

The purpose of this study is to determine the electrical effects at the zirconia/oxygen interface. Specifically, in this paper we report the surface electrical effects accompanying oxidation of zirconia involving bulk specimens and thin films. These effects were determined using high temperature Kelvin probe that allows to measure work function changes at elevated temperatures and under controlled gas phase composition.

Work function

Work function (WF) is the electrical property that is extremely sensitive to the properties of the outermost crystal layer on an atomic level.

1418–2874/99/ $ 5.00
© 1999 Akadémiai Kiadó, Budapest
Akadémiai Kiadó, Budapest
Kluwer Academic Publishers, Dordrecht

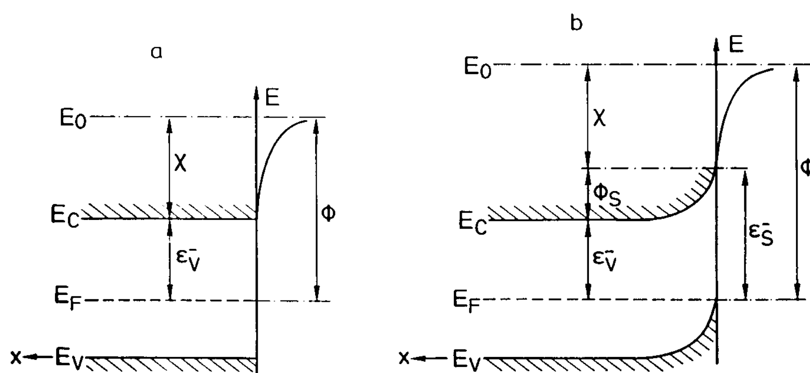

Fig. 1 The band model of a *p*-type semiconductor: a – free of surface charge, b – involving surface charge

WF is the energy required to remove electron from the Fermi energy level to infinity. Figure la illustrates the band model of a *p*-type semiconductor surface without a surface charge. In this case, the WF (Φ) includes a component related to the Fermi energy, ε_v^-, (which also is termed the internal WF), and external WF, χ. For a charged surface (e.g., due to the presence of chemisorbed species), the WF involves an additional component, Φ_s, corresponding to the surface charge (Fig. lb). Assuming that there are no dipoles at the surface the WF asses the following form:

$$\Phi = \varepsilon_v^- + \Phi_s + \chi \quad (1)$$

The most convenient method of measuring the WF of solids at elevated temperatures is based on the dynamic condenser method. This method, initially proposed by Kelvin [5], has been substantially improved [6–9].

The principle of the Kelvin method is based on the measurements of the contact potential difference (CPD) that is formed between two surfaces forming a condenser; one of them is the studied surface, of which WF is Φ_2, and a reference surface, of which WF is Φ_1:

$$e(CPD) = \Phi_2 - \Phi_1 \quad (2)$$

Accordingly:

$$\Phi_2 = \Phi_1 + e(CPD) \quad (3)$$

Later modifications of the Kelvin probe included introduction of continuous vibration of the condenser, resulting in the generation of a continuous a.c. signal, and the automatic compensation of the CPD [7–9] .

Figure 2 shows a schematic illustration of a high-temperature Kelvin probe involving a vibrating condenser located in a reaction chamber where both temperature and $p(O_2)$ are controlled and the electronic set-up is based on a lock-in amplifier.

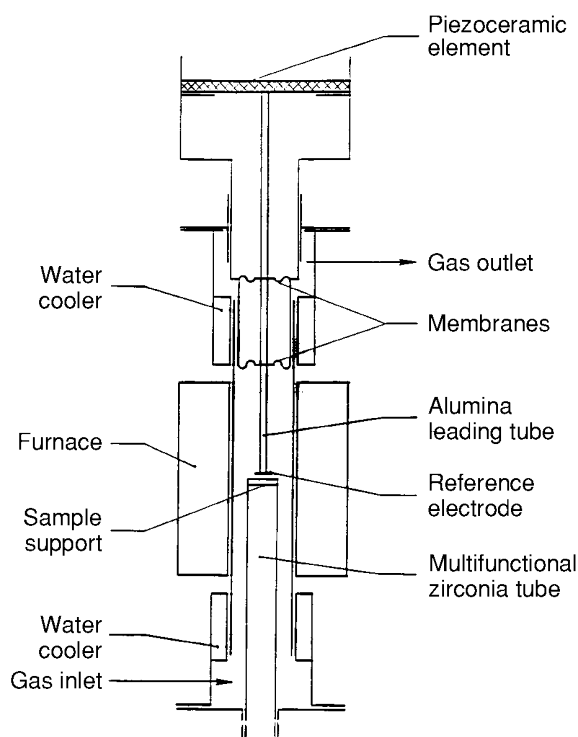

Fig. 2 Schematic illustration of a high-temperature Kelvin probe

The principle of the Kelvin probe and its applications in the study of surface properties of metal oxides at elevated temperatures and under controlled gas phase compositions have been reported in ref. [9].

The construction of High-Temperature Kelvin Probe, that enables WF measurements at elevated temperatures, is described in ref. [9] (Fig. 2). This construction allows operation up to 1000°C under controlled oxygen partial pressure.

The main signal, which is generated by the vibrating capacitance, may be measured with sufficient accuracy only when the level of external noise is limited to a minimum. Accordingly, careful screening of the condenser from noise signals is required.

As seen from Eq. (1), the absolute value of WF for a surface of an ionic solid has a complex physical meaning and involves three different components (assuming that changes of the dipole moment during interaction of a gas phase component with an oxide surface can be neglected). Assuming that the structure of the outermost surface layer rennains unchanged (χ=const), then WF changes are determined by only two components:

$$\Delta\Phi = -\Delta E_F + \Delta\Phi_s \tag{4}$$

where ΔE_F is the WF component determined by changes in crystal composition (non-stoichiometry) and resultant changes in the Fermi energy level, E_F, where:

$$(\Delta\Phi)_s = -(\Delta E_F)_s \tag{5}$$

The subscript *s* in Eq. (5) concerns surface layer.

Depending on the experimental procedure one of these two components is predominant. In the case of an oxide/oxygen system, the component ΔE_F is predominant at high temperatures when changes in $p(O_2)$ result in immediate changes in oxide non-stoichiometry. However, at lower temperatures (below equilibrium), the changes in WF due to variations in $p(O_2)$ are determined by the changes in surface coverage by chemisorbed oxygen species.

When metal oxide remains in equilibrium with the gas phase then the following relationships for the concentration of electronic charge carriers may be written:

$$n = N_C \exp[(E_F - E_C)/kT] \tag{6}$$

$$p = N_V \exp[(E_V - E_F)/kT] \tag{7}$$

$$n, p = \text{const}\, p(O_2)^{1/n} \tag{8}$$

where *n* is quantity that has been used in verification of defect chemistry models [10–13]. Concordantly, the $p(O_2)$ WF dependence may be expressed by the following expression:

$$\frac{1}{n_\Phi} = \frac{1}{kT}\frac{\partial\Phi}{\partial \ln p(O_2)} \tag{9}$$

The set of Eqs (6)–(9), and specifically the parameter n_Φ in Eq. (9), allow to evaluate the $p(O_2)$ dependence of electrical properties that can be used to verify defect models. The electrical properties based on WF data can be used to determine defect model for the surface layer rather than for the bulk phase.

By analogy with other electrical properties, the WF data taken at the gas/solid equilibrium are well defined and may be considered as material data that are characteristic of the material under study. According to Eq. (9), the WF value measured in equilibrium is determined by the parameters describing the equilibrium, such as temperature and oxygen partial pressure. Then WF is independent of the experimental procedure applied.

Preparation

Bulk specimens

Polycrystalline yttria-stabilised (10 mol%) zirconia, provided by Tosoh Co. , was first uniaxially pressed into discs (diameter – 10 mm, thickness – 2 mm), then isostatically pressed under 200 MPa at room temperature, sintered at 1673 K for 2 h

and finally isostatically pressed again at 1473 K under 200 MPa for 1 h. The relative density of the specimens was 99.8% and grain size 2–3 μm.

Sintered specimens were cleaned with acetone, polished with 0.25 μm diamond powder, cleaned with acetone in ultrasonic bath, polished again and then annealed for 2 h in air at 1473 K.

Thin films

The zirconia thin films were deposited using a CVD method. The $Zr(O{\cdot}t–C_4H_9)_4$ vapour was generated by bubbling nitrogen through liquid and $Y(C_{11}H_{19}O_2)_3$ vapour was formed through heating and passing nitrogen. The mixture of both vapours and oxygen (under 1330 Pa) was then introduced into a CVD reactor, through a nozzle, involving substrates made of yttria-doped zirconia pellets. The temperature of the substrate was 873 K.

Experimental procedure

The gas phase in the reaction chamber was imposed by air (oxidation) and argon (reduction) flowing through the reaction chamber at a flow rate of 100 ml min^{-1}. The respective oxygen partial pressure was $2.1{\cdot}10^4$ and 13.7 Pa.

Before each measurement, the specimen was heated to 1173 K in argon at a rate of 400 K h^{-1} annealed at 1173 K in Ar for 2 h and then cooled down, with the same rate, to the temperature of the experiment in the range 297–1173 K. The oxidation experiments involved an increase of oxygen pressure from 13.7 Pa to $2.1{\cdot}10^4$ Pa. Then the CPD changes, caused by oxidation, were determined.

Results and discussion

The CPD changes during oxidation can be considered as a certain measure of chemical affinity between the zirconia surface and oxygen. The bulk component of this change is determined by the change of oxygen non-stoichiometry and related changes in Fermi energy. The surface component of the CPD change, that corresponds to the surface charge, is determined by surface coverage with chemisorbed species and their valency.

Figures 3 and 4 show the CPD changes caused by change in $p(O_2)$ during oxidation for the bulk zirconia specimen, named as standard specimen, (curve 1), for the thin film of undoped zirconia (curve 2, Fig. 3) and yttria-doped zirconia (curve 2, Fig. 4). Since the temperature of films deposition was 873 K, the highest temperature applied for the WF measurements was also 873 K.

As seen the ΔCPD for the standard zirconia assumes two maxima. The maximum at 373 K, that corresponds the state below equilibrium [13], is about 130 mV. The maximum at 973 K, that corresponds to equilibrium of the zirconia/oxygen system [13], is twice larger.

The maximum for undoped zirconia film at 373 K (curve 2 in Fig. 3) is twice larger than that for the standard zirconia (curve 1 in Fig. 3) and is shifted to 473 K.

After assuming minimum at 623 K an increase of the ΔCPD with increase of temperature can be observed. Entirely different picture is observed for the thin film of zirconia stabilised with yttria. As seen from Fig. 4 addition of yttrium to the film results in a substantial reduction of ΔCPD at 373 K (curve 2 in Fig. 4), in comparison to that of standard specimen (curve 1 in Fig. 4). Maximum of the ΔCPD for the thin film involving yttria is at 600 K and then has a tendency to decrease with temperature.

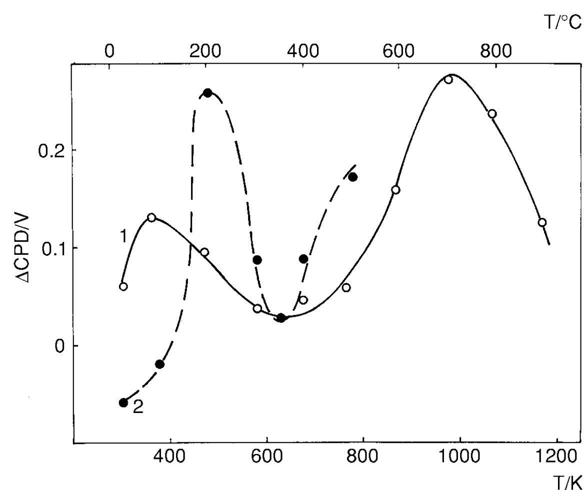

Fig. 3 The CPD changes during isothermal oxidation; 1 – standard (bulk) zirconia involving 10 mol% Y_2O_3, 2 – undoped ZrO_2 thin film

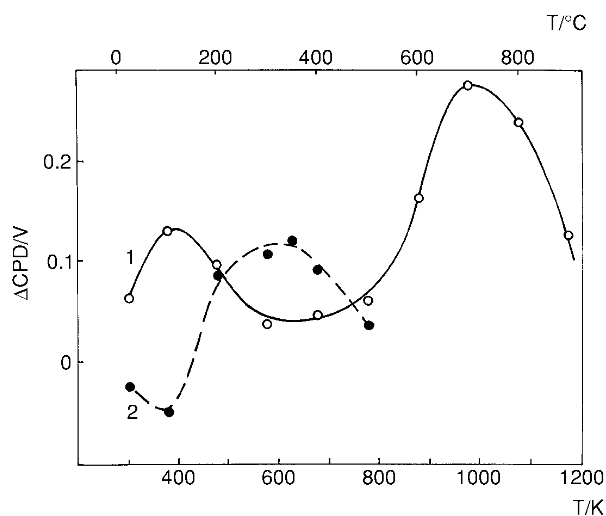

Fig. 4 The CPD changes during isothermal oxidation; 1 – standard (bulk) zirconia involving 10 mol% Y_2O_3, 2 – ZrO_2+Y_2O_3 (10 mol%) thin film

Conclusions

The standard zirconia specimen exhibits two maxima of ΔCPD; one at 373 (below equilibrium) and at 973 K (in equilibrium). This 373 K maximum corresponds to maximum of oxygen chemisorption isobar. The 973 K maximum indicates that at this temperature oxidation results in the formation of the surface charge that is related to the presence of chemisorbed oxygen species. This charge decreases at higher temperatures.

For undoped ZrO_2 film the maximum of oxygen isobar is shifted to 473 K, assumes minimum at 623 K and then has a tendency to increase at higher temperatures. In the case of the thin film containing Y_2O_3 the picture is entirely different. The initial maximum of ΔCPD appears at 600 and then, above 600 K, has a tendency to decrease suggesting that the charge build-up for thin film is lower than that for the bulk material.

References

1 D. Hennings, in: 'Surface and Near-Surface Chemistry of Oxide Materials', J. Nowotny and L. C. Dufour, Eds., Elsevier, Amsterdam, 1988, p. 479.
2 J. Nowotny, in: 'Science of Ceramic Interfaces', Elsevier, Amsterdam 1981, p. 7.
3 J. Nowotny, in: 'Science of Ceramic Interfaces II', Elsevier, Amsterdam, 1991 p. 1 & 663.
4 N. Mizutani and J. Nowotny, in: 'Ceramic Interfaces', S. J. L. Kang and H. I. Yoo, Eds., The Institute of Materials, London (in press).
5 Kelvin (Lord), Phil. Mag., 46 (1898) 82.
6 W. A. Zisman, Rev. Sci. Instr., 3 (1932) 367.
7 J. C. P. Mignolet, Disc. Farad. Soc., 8 (1950) 326.
8 R. Chrusciel, J. Deren and J. Nowotny, Exp. Techn. Phys., 14 (1966) 127.
9 K. Besocke and S. Berger, Rev. Sci. Instr., 47 (1976) 840.
10 J. Nowotny, M. Sloma and W. Weppner, Adv. Cer., 23 (1987) 159.
11 P. Kofstad, in: 'Nonstoichiometry, Diffusion and Electrical Conductivity of Binary Metal Oxides', Wiley, 1972.
12 P. Odier, J. C. Riflet and J. P. Loup, Mattr. Sci. Monographs #10, Esevier, 1982, p. 458.
13 K. Mukae, T. Bak, X. Li, N. Mizutani, J. Nowotny, A. Saiki, C.C. Sorrell and Z. Zhang, J. Austral. Cer. Soc., 34 (1998) 76.